Functional Characterization of Nitric Oxide and YC-1 Activation of Soluble Guanylyl Cyclase: Structural Implication for the YC-1 Binding Site?†

Maria Lamothe,‡ Fu-Jung Chang,‡ Nataliya Balashova, Roman Shirokov, and Annie Beuve*

Department of Pharmacology and Physiology, New Jersey Medical School, University of Medicine and Dentistry of New Jersey, 185 South Orange Avenue, Newark, New Jersey 07103

Received November 10, 2003; Revised Manuscript Received December 12, 2003

ABSTRACT: Soluble guanylyl cyclase (sGC) is a heterodimeric enzyme formed by an α subunit and a β subunit, the latter containing the heme where nitric oxide (NO) binds. When NO binds, the basal activity of sGC is increased several hundred fold. sGC activity is also increased by YC-1, a benzylindazole allosteric activator. In the presence of NO, YC-1 synergistically increases the catalytic activity of sGC by enhancing the affinity of NO for the heme. The site of interaction of YC-1 with sGC is unknown. We conducted a mutational analysis to identify the binding site and to determine what residues were involved in the propagation of NO and/or YC-1 activation. Because guanylyl cyclases (GCs) and adenylyl cyclases (ACs) are homologous, we used the three-dimensional structure of AC to guide the mutagenesis. Biochemical analysis of purified mutants revealed that YC-1 increases the catalytic activity not only by increasing the NO affinity but also by increasing the efficacy of NO. Effects of YC-1 on NO affinity and efficacy were dissociated by single-point mutations implying that YC-1 has, at least, two types of interaction with sGC. A structural model predicts that YC-1 may adopt two configurations in one site that is pseudosymmetric with the GTP binding site and equivalent to the forskolin site in AC.

The soluble guanylyl cyclase (sGC) is the predominant receptor for nitric oxide (NO)[1] and mediator of most of its effects. The sGC is a heme-containing heterodimeric enzyme formed by an α subunit and a β subunit. Histidine 105 (H105) of the β_1 subunit coordinates the heme at which NO binds (*1*). When NO binds, the basal catalytic activity of sGC increases several hundred fold to produce the second-messenger cGMP from the substrate GTP (*2*, *3*). It is generally accepted that binding of NO to the heme induces cleavage of the His−heme bond, which in turn creates a conformational change that results in stimulation of the catalytic activity (*4*). However, no residue of the sGC has been identified as being involved in the downstream structural changes that follow the NO−heme interaction.

A synthetic compound, YC-1, was shown to synergistically activate the sGC in the presence of NO, apparently by slowing the rate of dissociation of NO from the heme (*5*, *6*). Indeed, the EC_{50} for activation by NO is lowered by 1 order of magnitude in the presence of YC-1, suggesting that YC-1 increases the affinity of NO for the heme (*7*, *8*). YC-1 can also activate sGC independently of NO by an unknown mechanism (*9*, *10*). Attempts to identify in sGC the site(s) of allosteric regulation by YC-1 or its derivatives have recently intensified but have had limited success (*11, 12*), and no residue has been identified as participating in the conformational change that accompanies YC-1 binding.

Guanylyl cyclases (GCs) have several functional and structural features in common with adenylyl cyclases (ACs) (*13*). Both classes of enzymes catalyze the cyclization of chemically related substrates, GTP and ATP. Binding and catalysis occur in the COOH-terminal part of the α and β subunits of sGC and in the C_1 and C_2 cytoplasmic domains of ACs. These regions of ACs and GCs are homologous in their primary structure (*14*). Association of C_1 and C_2 domains of ACs and α and β subunits of sGC is required for catalytic activity.

A breakthrough in understanding the structure and function of the cyclase family occurred when the crystal structure of a catalytically active form of an AC was determined (*15*). A head-to-tail association between the cytoplasmic C_1 and C_2 domains of the ACs creates a region in a shape of a shallow trough that defines the interface. At this interface, two binding pockets are formed and extensive contacts between the two domains occur. One pocket is the substrate binding site where ATP binds and catalysis takes place. The other is the regulatory site at which forskolin (FSK), an allosteric activator of the AC, binds. This FSK binding pocket is pseudosymmetric with the ATP binding pocket. This structural organization is illustrated in the scheme of Figure 1.

† This work was supported by American Heart Association Grant SDG 0130506T, the Foundation of the University of Medicine and Dentistry of New Jersey, and NIH Grant RO1-GM067640 (A.B.). R.S. is supported by NIH Grant RO1-MH 62838.

* To whom correspondence should be addressed. Phone: (973) 972-8838. Fax: (973) 972-4554. E-mail: annie.beuve@umdnj.edu.

‡ These authors contributed equally to this work.

[1] Abbreviations: NO, nitric oxide; YC-1, 1-benzyl-3-(hydroxymethyl-2-furyl)indazole; FSK, forskolin; $G_{s\alpha}$, subunit of the G protein G_s; SNP, sodium nitroprusside; Glyco-SNAP-2, *N*-(β-D-glucopyranosyl-N_2-acetyl-*S*-nitroso-D,L-penicillaminamide); IBMX, 3-isobutyl-1-methylxanthine; DMEM, Dulbecco's modified Eagle's medium; PAGE, polyacrylamide gel electrophoresis; β-ME, β-mercaptoethanol; EDTA, ethylenediaminetetraacetic acid; EGTA, ethylene glycol bis(β-aminoethyl ether)-*N*,*N*,*N*′,*N*′′-tetraacetic acid; HEPES, 4-(2-hydroxyethyl)-1-piperazineethanesulfonic acid; PMSF, phenylmethanesulfonyl fluoride.

10.1021/bi0360051 CCC: $27.50
Published on Web 02/24/2004

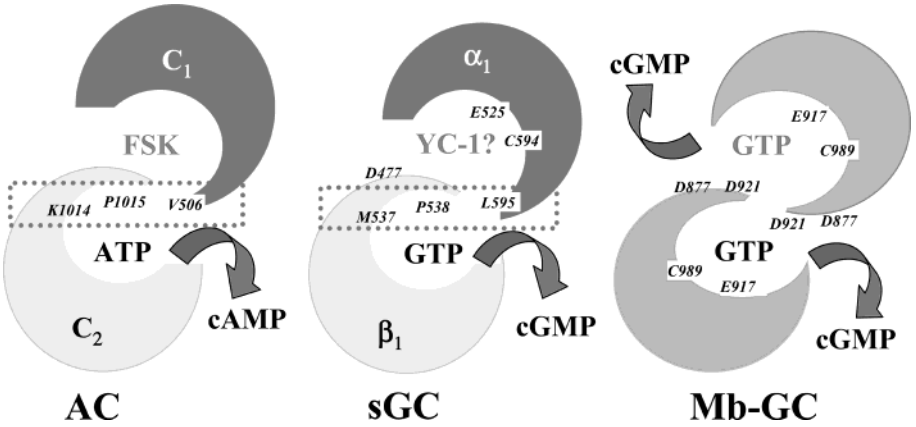

FIGURE 1: Scheme of the catalytic core of adenylyl cyclase (AC), soluble guanylyl cyclase (sGC), and membrane-bound guanylyl cyclase (Mb-GC). The interface residues from AC and the corresponding sGC residues are boxed. Residues in Mb-GC predicted to be involved in GTP catalysis are numbered according to the rat GC-A amino acid sequence.

Modeling of sGC revealed a similar structural organization (*14*). The association of the COOH termini of both α and β subunits results in the formation of the GTP binding pocket and a putative second pocket that corresponds to the FSK site of AC. This second pocket is homologous with the GTP binding pocket but lacks residues that are critical for substrate catalysis (*16*). This second pocket is pseudosymmetric with the GTP binding pocket, as shown in Figure 1.

The structural homology of AC and sGC suggests that these two enzymes are functionally similar. This leads to the idea that the pseudosymmetric binding pocket of sGC has an allosteric function similar to that of the FSK binding pocket of AC. If so, it is a logical site for YC-1 binding (*17*). Unlike those with heterodimeric sGCs, kinetic studies with homodimeric membrane-bound GCs had suggested two cooperative GTP binding sites (Figure 1; *18*−*20*). YC-1 is structurally homologous with nucleoside, further supporting the hypothesis that the pseudosymmetric binding pocket of the sGC contains the YC-1 binding site.

One prevalent model of FSK action is one in which the C_1 and C_2 domains of AC are only loosely associated in the absence of stimulation but binding of FSK promotes a more favorable conformation for the active site by increasing the affinity between C_1 and C_2 at the contact regions of the interface (*15*, *21*). A recent mutational analysis supports this model (*22*). The residues and secondary structures that shape the interface between the C_1 and C_2 domains are conserved in the α_1 and β_1 subunits of the sGC, suggesting that contacts at the subunit interface are critical for transduction of YC-1 and NO signals of activation (boxed residues in Figure 1).

On the basis of these homologies within the cyclase family, we conducted a mutational analysis of the putative YC-1 binding pocket and of contacts at the interface between the two subunits. We describe herein the biochemical consequences of these mutations and propose, as a working hypothesis, a structural model of the interaction of YC-1 with the sGC.

EXPERIMENTAL PROCEDURES

Mutagenesis and Transfection in COS-7 Cells. Templates were cDNAs encoding the α_1 and β_1 subunits of rat sGC cloned into the mammalian expression vector pCMV5 (*23*). Mutations were introduced by PCR (Quickchange, Stratagene). Sequences of sense and antisense primers are available upon request. COS-7 cells were grown in DMEM supplemented with 10% heat-inactivated fetal bovine serum (FBS), penicillin, and streptomycin (100 units/mL). Cells were transfected with PolyFect reagent using the protocol of the supplier (Qiagen).

Measurement of cGMP Production in Intact COS-7 Cells. COS-7 cells were plated in 24-well plates and transfected at 80−90% confluency with 1.0 μg each of plasmids encoding wild-type (WT) or mutant α_1 and β_1 subunits. After 46 h, cells were placed at room temperature and washed once with warm phosphate-buffered saline and once with warm serum-free DMEM. DMEM containing 10% heat-inactivated FBS, 50 mM NaHEPES (pH 7.4), and 1 mM 1-methyl-3-isobutylxanthine (IBMX, an inhibitor of cyclic nucleotide phosphodiesterases) was added to each well in duplicate; 180 μL of this medium was added to the wells that received 20 μL of DMEM, 20 μL of 10 mM sodium nitroprusside (SNP), or 20 μL of 1 mM YC-1, whereas 160 μL of the medium was added to the wells receiving 20 μL of 10 mM SNP and 20 μL of 1 mM YC-1. Plates were then warmed to 37 °C for 15 min. The incubation was terminated by adding 15 μL of 33% perchloric acid. The amount of cGMP in the perchlorate extract was measured by radioimmunoassay (*24*) after neutralization with 15 μL of 10 N potassium hydroxide. The cGMP content was determined in three separate experiments (three independent transfections, each in duplicate) with similar results.

Preparation of COS-7 Cytosols. Cells (100 mm dish) were transfected with 6 μg of the α_1 wild-type or mutated subunit and 4 μg of the β_1 wild-type or mutated subunit. After 46 h, cells were washed four times with 8 mL of ice-cold Puck's Saline G (137 mM NaCl, 54 mM KCl, 1.1 mM KH_2PO_4, and 1.1 mM Na_2HPO_4) and sonicated in 350 μL of homogenization buffer [50 mM Tris-HCl (pH 8.0) at 4 °C, 150 mM NaCl, 10% glycerol, and protease inhibitors]. The cytosolic fraction was collected by centrifugation at 100000*g* for 20 min at 4 °C.

Baculovirus Construction. Oligonucleotide primers encoding the NH_2 and COOH termini of α_1 and β_1 wild-type (WT) or mutated subunits were used for subcloning the corresponding cDNA by PCR. The NH_2-terminal oligonucleotides incorporated the initiating methionine of each isoform, and the COOH-terminal oligonucleotides contained sequences encoding the stop codon. For His-6-tagged versions of the

β_1 subunit, COOH-terminal primers contained a glycine and six histidines followed by a stop codon. The resulting PCR fragments were inserted into baculovirus transfer vector pBacPAK8. Viruses were generated by homologous recombination following cotransfection of BacPAK6 viral DNA (Bsu36 I digest, Clontech).

Expression and Purification of sGC and Mutants. The α_1/β_1-His_{tag} sGC and mutants were expressed using the Sf21/baculovirus system. High-titer virus stocks were obtained from the Sf21 suspension culture harvested 72 h after infection. Five hundred milliliters of Sf21 cells (1.5×10^6 cells/mL) were co-infected with α_1- and β_1-His_{tag}-containing viruses (ratio 3:1) and grown for 48 h. Cells were harvested by centrifugation at 1500*g* for 10 min. All subsequent steps were carried out at 4 °C. The pellet was resuspended in 25 mL of ice-cold phosphate-buffered saline (PBS) containing protease inhibitors [PIs, 10 μg/mL leupeptin, 10 μg/mL aprotinin, and 35 μg/mL phenylmethanesulfonyl fluoride (PMSF)] and disrupted with a Dounce homogenizer. The homogenate was centrifuged at 100000*g* for 1 h. The supernatant fraction was passed through 1 mL of Talon cobalt resin (Clontech) equilibrated with 10 mL of PBS containing PIs and 0.015% β-mercaptoethanol (β-ME). The column was washed according to the supplier's instruction. Proteins were eluted with 50 mM NaCl, 50 mM EDTA, and 20 mM Tris (pH 8.0) containing 0.015% β-ME, and 0.5 mL fractions were collected. Fractions with the highest protein concentration were pooled and after dilution in buffer A [2 mM $MgCl_2$, 1 mM EDTA, 1 mM DTT, and 20 mM HEPES (pH 8.0)] applied to a Mono Q HR 5/5 column (Pharmacia) at 1 mL/min. Proteins were eluted with increasing concentrations of NaCl. Fractions with the highest sGC activity were pooled in 10% glycerol and 5 mM DTT and snap-frozen. Protein concentrations were determined as described previously (*25*). Purified preparations of the sGC and mutants were resolved on a 10% SDS−PAGE gel and stained with Colloidal Coomassie Blue (Pierce) (see the Supporting Information).

Assay of GC Activity. GC activity was determined as previously described (*24*). In short, assays were performed in a volume of 100 μL for 10 min at 30 °C. The final concentration of GTP was 500 μM in a reaction buffer containing 50 mM HEPES (pH 8.0), 1 mM DTT, and 4−5 mM $MgCl_2$. For measurement of GC activity in cytosolic fractions, 250 μM IBMX was added to the reaction buffer. Specific GC activity was measured in the absence of an activator (basal condition) or in the presence of 100 μM Glyco-SNAP-2, 100 μM YC-1, or both, unless otherwise stated. The effect of YC-1 on maximal NO-stimulated activity was calculated by dividing the activity obtained in the presence of both NO and YC-1 (less YC-1 stimulated activity) by the maximal NO-stimulated activity. The statistical significance of the ratio (difference between maximal NO-stimulated activity in the presence or absence of 100 μM YC-1) was assessed by a paired *t* test from four experiments carried out in duplicate.

K_m and V_{max} were determined with substrate concentrations ranging from 10 to 1000 μM, in the absence of activator, in the presence of 1 μM Glyco-SNAP-2 or 100 μM YC-1, and in the presence of the combination of 1 μM Glyco-SNAP-2 and 100 μM YC-1. The concentration of free magnesium was kept constant at 4 mM. All assays were performed in duplicate, and each experiment was repeated three times.

For Glyco-SNAP-2 and YC-1 concentration−response curves of the purified WT and mutants, GC activity was measured in the presence of 10 different concentrations of Glyco-SNAP-2 (from 0.01 to 300 μM) and eight increasing concentrations of YC-1 (from 0.1 to 300 μM). The Glyco-SNAP-2 concentration−response curves were similarly established in the presence of 10 and 100 μM YC-1. All concentration−response experiments were performed in duplicate, and each experiment was repeated two or three times and with two independently purified WT and mutant enzymes (four to six independent experiments). The EC_{50} values were calculated from the dose−response curves that were representative of these four to six independent experiments and corresponded to the concentration of Glyco-SNAP-2 that half-maximally activates the enzyme. An *F* test that compares the NO concentration−response curves in the absence or presence of YC-1 was combined with a paired *t* test to determine the significance of the difference between the EC_{50} obtained with or without YC-1.

The effect of YC-1 on maximal NO-stimulated activity was also calculated from the plateau of the various concentration−response curves. A paired *t* test was used to determine if the difference in the maximal NO-stimulated activity in the absence or presence of 10 and 100 μM YC-1 was statistically significant. The data points of the NO concentration−response curves that constituted a plateau (typically at 30, 100, and 300 μM Glyco-SNAP-2) were grouped for statistical analysis and tested against the same group of data points obtained in the presence of YC-1 (a *P* of <0.05 was considered statistically significant).

Reagents. Reagents and nucleotides were purchased from Sigma Chemical and Boehringer-Mannhein, at the highest purity grade available. YC-1 was synthesized and kindly provided by V. Collot in S. Rault's group (CERM, University of Caen, Caen, France) (*26*). YC-1 and BAY 41-2272 (Calbiochem) were dissolved in dimethyl sulfoxide (DMSO). The final concentration of DMSO was less than 0.1% in the reaction mix. Except for initial screening in intact COS-7 cells, Glyco-SNAP-2 rather than SNP was used as an NO donor because it releases NO at a more constant rate and for a longer period of time (according to the description from the supplier, Calbiochem).

Homology-Based Molecular Modeling. For the modeling, coordinates of the AC atoms were downloaded from the RCSB Protein Data Bank (entry 1azs). The following parts of the rat sGC amino acid sequences were used: α_1V480−L625, β_1V420−L485, and β_1H492−E576. Homology, Biopolymer, and Discover modules of the Insight II molecular modeling software bundle (Accelrys, San Diego, CA) were used. The starting conformation was built assuming the coordinates of the sGC atoms are similar to those of the AC. Water molecules were added to make a 5 Å thick layer. The total number of atoms at this stage was 9507. Atom−atom interactions were calculated using the extensible systematic force field (esff) approximation. Energy minimization was carried out by the conjugate gradient method until the maximum derivative was less than 0.001 kcal mol^{-1} $Å^{-1}$. Ligand docking was performed in two steps. First, GTP, YC-1 molecules, and Mg^{2+} ions were manually positioned in the catalytic and apparent regulatory sites of the sGC. Then the energy was minimized with all generalized coordinates allowed to vary.

Table 1: cGMP Production of Wild-Type Guanylyl Cyclase and Mutants in Intact COS-7 Cells[a]

	cGMP production in intact cells (pmol/well)			
	with SNP	with YC-1	with SNP and YC-1	phenotype
α_1/β_1	8.2 ± 1.3	2.3 ± 0.8	11.5 ± 1.1	
α_1C238S/β_1	9.2 ± 0.3	2.1 ± 0.3	11.6 ± 1.4	unchanged
α_1C243S/β_1	7.8 ± 0.2	3.1 ± 0.3	11.1 ± 1.3	unchanged
α_1C238S-insert-C243S/β_1 putative YC-1 allosteric site	7.9 ± 0.3	3.2 ± 0.7	12.4 ± 0.9	unchanged
α_1C594D-E525K/β_1	1.2 ± 0.5	0.6 ± 0.1	2.2 ± 0.5	mostly lost all activities
α_1C594D/β_1	4.4 ± 1.3	0.5 ± 0.1	4.6 ± 1.3	no YC-1 activation, no synergy
α_1C594Y/β_1	1.2 ± 0.4	0.6 ± 0.2	5.8 ± 1.0	reduced level of NO and YC-1 activation, synergy
α_1/β_1D477A potential interface contact	2.9 ± 0.7	0.7 ± 0.2	7.1 ± 1.6	reduced level of NO and YC-1 activation, synergy
α_1/β_1M537N	7.4 ± 0.9	3.5 ± 0.4	6.9 ± 0.4	high level of YC-1 activation, no synergy

[a] The cGMP production in intact cells was measured by RIA after stimulation by 1 mM SNP, 100 μM YC-1, and 1 mM SNP with 100 μM YC-1. Data are means ± the standard error of the mean of three experiments.

RESULTS

Site-Directed Mutagenesis. To probe the site that potentially interacts with YC-1, we introduced mutations in the pseudosymmetric pocket that corresponded to residues that are critical for catalysis in the substrate binding pocket (*27*). The replacement in the α_1 subunit of cysteine 594 with tyrosine and aspartate, and of glutamate 525 with lysine, generated mutants α_1C594Y/β_1 and α_1C594D/β_1 and the double mutant α_1C594D-E525K/β_1. α_1/β_1D477A was generated by replacing aspartate 477 of the β_1 subunit because the equivalent aspartate in the α_1 subunit (D531) is thought to coordinate the metal ion of the substrate Mg^{2+}GTP, like in ACs (*15*, *28*).

At the interface, methionine 537 of β_1 was replaced with asparagine (α_1/β_1M537N). This mutant corresponded to the AC interface mutant (C_1/C_2K1014N) that is critical for the propagation of FSK and $G_{s\alpha}$ activation (*22*).

All residues mentioned above are invariant in the known mammalian amino acid sequences of sGCs that respond to YC-1 and NO activation (*29*).

Recent work using a photoactivated derivative of YC-1 suggested the involvement of cysteines 238 and 243 of the α_1 subunit in YC-1 binding (*11*). However, these cysteines are not conserved in the sGC α_1 subunit of other species (*12*, *29*), are located outside the catalytic core of the sGC, and outside the region of homology with AC. Nevertheless, these two cysteines were replaced, and additionally, 13 amino acids were randomly inserted between the mutated cysteines (C_{238}SFRSESTEFVMPPSFRSEC_{243}S).

cGMP Production in Intact Cells. Wild-type (WT) and mutated cDNAs were transfected into COS-7 cells, and their cGMP content was measured by radio-immunoassay (RIA) under the basal condition and after exposure to NO, to YC-1, or to both activators (Table 1). The three α_1C238S, α_1-C243S, and α_1C238S-insert-C243S mutants displayed a phenotype similar to that of the WT. In the pseudosymmetric pocket, α_1C594D-E525K/β_1 lost most responses whereas α_1-C594D/β_1 was not activated by YC-1, was still responsive to NO, and showed no synergy in the presence of NO and YC-1. Interestingly, α_1C594Y/β_1, and α_1/β_1D477A lost response to YC-1 and exhibited a weak response to NO but displayed a stronger response when both activators were present. Interface mutant α_1/β_1M537N had a strong response to YC-1 but no additive effect in the presence of both NO and YC-1 (Table 1).

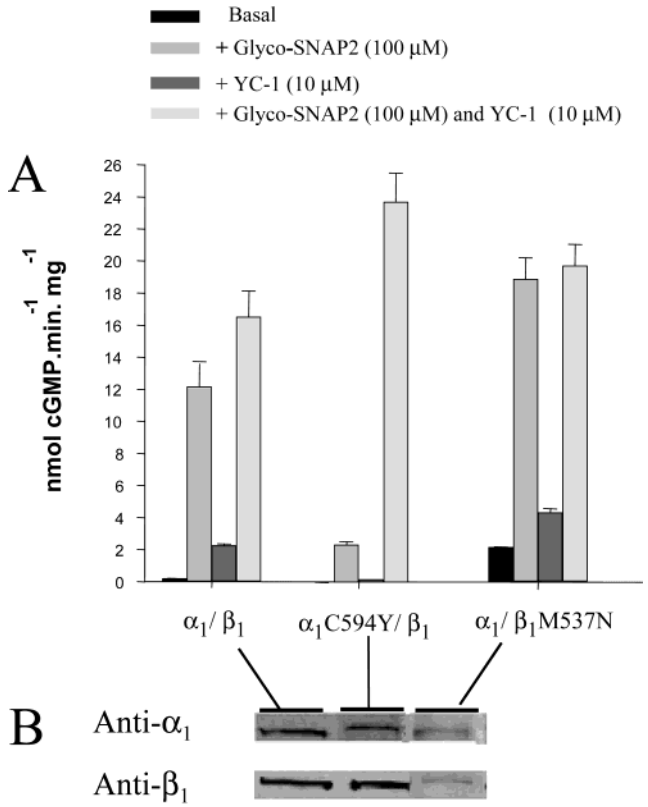

FIGURE 2: (A) Guanylyl cyclase activity in COS-7 cytosols of the WT and selected mutants was assessed in the absence of an activator and in the presence of 100 μM Glyco-SNAP-2, 10 μM YC-1, or both. No GC activity was detected in untransfected COS-7 cells. These results are means ± the standard error of the mean of cytosols prepared from two separate tissue culture plates, which were assayed in duplicate. Data are representative of four independent experiments with similar results carried out with three different batches of transfected cells. (B) Western blot analysis of cytosols expressing the WT enzyme and selected mutants shows a lower level of expression of the α_1 and β_1 subunits in α_1/β_1M537N.

sGC Activity in Cytosols Expressing WT, α_1C594Y/β_1, and α_1/β_1M537N. In the cytosols of cells expressing WT, NO and YC-1 induced approximately 25- and 4-fold increases in basal activity, respectively (Figure 2). We detected only a slight increase in GC activity by simultaneous exposure to NO and YC-1. This increase is consistent with the small synergistic effect, at a saturating concentration of the NO donor, usually observed in cells that express endogenous sGC (*30*, *31*). Unfortunately, we could not detect GC activity in

Table 2: Characteristics of Purified Wild-Type Guanylyl Cyclase and Mutants[a]

(a) Specific Activities

	activity (nmol min^{-1} mg^{-1})				effect of YC-1 on maximal NO-stimulated activity (NO efficacy) (fold stimulation)
	basal	with Glyco-SNAP-2 (100 μM)	with YC-1 (100 μM)	with Glyco-SNAP-2 and YC-1 (100 μM each)	
α_1/β_1	119 ± 20	9110 ± 163	569 ± 22	12090 ± 600	1.3[b]
α_1C594Y/β_1	43 ± 11	4290 ± 66	116 ± 13	21500 ± 601	5.1[b]
α_1/β_1M537N	703 ± 53	34020 ± 2400	3198 ± 151	36700 ± 1150	1.0

(b) Kinetic Analysis

					effect of YC-1 on NO affinity EC_{50} (Glyco-SNAP-2) (μM)		
						with YC-1	
kinetic parameter	basal	with Glyco-SNAP-2 (1 μM)	with YC-1 (100 μM)	with Glyco-SNAP-2 and YC-1	without YC-1	10 μM	100 μM
α_1/β_1							
K_m	122 ± 11	61 ± 18	39 ± 4	25 ± 3	4.4	2.6[b]	1.0[b]
V_{max}	89 ± 7	1400 ± 225	413 ± 51	5076 ± 120			
α_1C594Y/β_1							
K_m	>400	84 ± 13	158 ± 19	48 ± 8	3.4	3.0	3.1
V_{max}	40 ± 1	689 ± 84	91 ± 3	7692 ± 315			
α_1/β_1M537N							
K_m	156 ± 5	124 ± 9	139 ± 1	36 ± 7	1.5	1.0	0.5[b]
V_{max}	605 ± 90	10570 ± 1100	2656 ± 311	21235 ± 2298			

[a] The apparent K_m is expressed in micromolar and V_{max} in nanomoles of cGMP per minute per milligram. EC_{50} values for activation by Glyco-SNAP-2 in the absence or presence of 10 and 100 μM YC-1 were determined from the plots of Figures 3 and 4. [b] Statistically significant ($P < 0.05$).

the cytosols of cells expressing α_1/β_1D477A and α_1C594D/β_1. In agreement with screening of intact cells, α_1C594Y/β_1 exhibited a weak response to NO and failed to produce a significant amount of cGMP in response to YC-1 alone but produced remarkably large amounts when both activators were present. In contrast, α_1/β_1M537N exhibited a strong response to NO and YC-1, but YC-1 lost the capacity to further enhance NO-stimulated cGMP production.

These mutations show that activation by individual ligands can be dissociated from activation by both ligands. To determine the mechanism for this effect, we purified WT, α_1C594Y/β_1, and α_1/β_1M537N and conducted a thorough biochemical analysis.

Kinetics Analysis of Purified WT, α_1C594Y/β_1, and α_1/β_1M537N. First, we compared the activity of the purified WT and mutant enzymes under the basal condition and at the maximal concentration of NO, YC-1, and both activators (Table 2a). The GC activity of WT (α_1/β_1) was maximally stimulated 76- and 5-fold by 100 μM Glyco-SNAP-2 and YC-1, respectively. In the presence of a saturating concentration of both activators, the activity was further increased by 1.3-fold ($P < 0.01$), as previously reported (*17*, *32*). The apparent K_m and V_{max} for GTP were determined by Lineweaver−Burk analysis under four different conditions [basal, 1 μM Glyco-SNAP-2, 100 μM YC-1, and both (Table 2b)]. The kinetic constants for GTP (K_m and V_{max}) were in the same range as previously reported values obtained under similar conditions (*7*, *32*−*34*).

α_1C594Y/β_1 Has Reduced Basal Activity and Lost Most YC-1 Activation, but YC-1 Tremendously Increases NO-Stimulated Activity. The α_1C594Y replacement reduced the basal activity by almost 3-fold (Table 2a). This mutation drastically increased the apparent K_m for GTP and decreased the apparent V_{max} (Table 2b). This basal phenotype was interesting as this residue, presumably located in the pseudosymmetric binding pocket, was not predicted to interfere with catalysis at the substrate binding pocket (in the absence of YC-1 activation). The specific activity in the presence of 100 μM Glyco-SNAP-2 was ~2-fold lower than that of the WT but still corresponded to a 100-fold increase over the basal activity. Addition of 1 μM Glyco-SNAP-2 increased the basal V_{max} in the same proportion as in WT and lowered the apparent K_m, indicating that the C594Y mutation did not affect the capacity of NO to induce a more favorable conformation for catalysis. In agreement with the initial screening in intact cells and cytosols, α_1C594Y/β_1 lost most responsiveness to YC-1, producing almost 5-fold less cGMP than the WT under the same conditions. This loss of response was reflected at the catalytic pocket by a K_m that was 4-fold higher and a V_{max} that was ~4-fold lower than those of the WT under the same conditions. A striking increase in catalytic activity was observed when NO and YC-1 were added simultaneously. The effect of YC-1 on maximal NO-stimulated activity corresponded to a 5.1 ratio ($P < 0.005$). This increase in catalytic activity appeared to be mainly due to an increase in the V_{max} of the reaction.

To investigate the mechanism underlying the opposite effects of YC-1 on basal and NO-stimulated activity, we established various concentration−response curves to both activators.

In WT, YC-1 Increases NO Affinity and NO Efficacy. We could not calculate an EC_{50} for activation by YC-1 for the WT or α_1C594Y/β_1 because a plateau could not be reached (inset of panels A and C of Figure 3), as previously observed (*9*). For the WT, the Glyco-SNAP-2 response curve (Figure 3A) corresponded to an EC_{50} for activation of 4.4 μM (Table 2b). YC-1 at concentrations of 10 and 100 μM shifted the NO response curve to the left, as shown in Figure 3A. This was reflected by a significant decrease in EC_{50} ($P < 0.01$; Table 2b), in agreement with previous studies (*8*, *17*). This

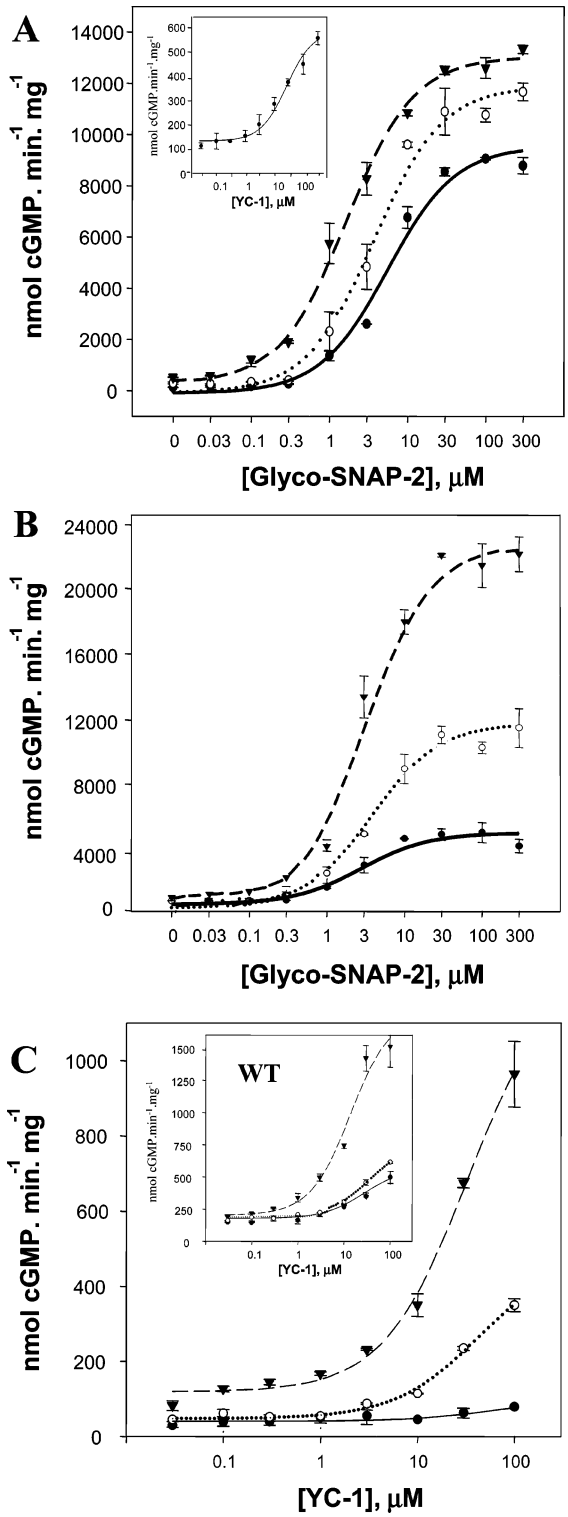

FIGURE 3: Glyco-SNAP-2 and YC-1 concentration−response curves of the purified WT and α_1C594Y/β_1. (A) α_1/β_1 Glyco-SNAP-2 concentration−response curves with or without YC-1 and (inset) YC-1 concentration−response curve. (B) α_1C594Y/β_1 Glyco-SNAP-2 concentration−response curves with or without YC-1. (C) α_1C594Y/β_1 YC-1 concentration−response curves with or without Glyco-SNAP-2 and (inset) the WT. Panels A and B: NO response curve (●) and NO response curve in the presence of 10 μM YC-1 (○) or 100 μM YC-1 (▼). Panel C: (●) YC-1 response curve and YC-1 response curve in the presence of 10 (○) and 100 nM Glyco-SNAP-2 (▼). Each experiment, carried out in duplicate, was repeated independently two or three times with two separate purified preparations, and results are the means ± the standard error of the mean of two experiments. Data are representative of these four to six independent experiments with similar results.

YC-1-induced decrease in EC_{50} for activation by NO indicates that YC-1 increases the affinity of NO for the heme (*5*, *7*). In addition, YC-1 at 10 or 100 μM was further able to significantly raise the plateau of maximal velocity of the NO-stimulated enzyme (Figure 3A; $P < 0.01$). Since Glyco-SNAP-2 is present at a saturating concentration, an increase in NO affinity cannot be responsible for the observed increase in catalytic activity. Therefore, YC-1 can also increase NO efficacy, as proposed in a recent study in intact cells (*35*).

In α_1C594Y/β_1, YC-1 Has No Effect on NO Affinity but Increases NO Efficacy. Consequently, we asked whether the remarkable increase in α_1C594Y/β_1 catalytic activity in the presence of YC-1 and Glyco-SNAP-2 was due to an enhanced capacity of YC-1 to increase NO affinity, NO efficacy, or both. In the absence of YC-1, the Glyco-SNAP-2 response curve (Figure 3B) corresponded to an EC_{50} for NO that was slightly lower than that of the WT, indicating that this mutation did not affect the response to NO. Most importantly, in the presence of 10 and 100 μM YC-1, the EC_{50} value for activation by Glyco-SNAP-2 was not significantly reduced ($P > 0.1$) while the maximal velocity, at a saturating concentration of NO, disproportionately increased (Figure 3B). These results indicated, first, that the enhanced affinity of NO cannot account for the synergistic increase and, second, that YC-1's capacity to increase NO efficacy is highly enhanced by the α_1C594Y mutation.

Because YC-1 can increase the catalytic activity only in the presence of Glyco-SNAP-2, we asked whether NO could reversibly potentiate YC-1-stimulated activity. When we measured responses of this mutant to YC-1 in the presence of submaximal concentrations of Glyco-SNAP-2, we observed an increase in activity larger than that of the WT (panel C and inset of Figure 3). From a YC-1 concentration of 10 μM or higher, Glyco-SNAP-2 at 10 and 100 nM increased activity by approximately 5- and 14-fold, respectively (vs less than 2- and 6-fold for the WT, respectively).

α_1/β_1M537N Displays a Constitutively Active Phenotype but No Synergism in Response to NO and YC-1. The interface mutant produced 6-fold more cGMP than WT under the basal condition. This high basal activity correlated with an increase in the V_{max} of the reaction rather than a change in the affinity for the substrate GTP (Table 2). Addition of 100 μM Glyco-SNAP-2 resulted in a specific activity of 34 020 nmol min^{-1} mg^{-1}. In response to YC-1, α_1/β_1M537N activity increased by 4.5-fold over an already high basal activity. In contrast to cytosolic preparations, the stimulated activities of the purified mutant were higher than those of the WT. By Western blot analysis, we observed that the α_1 subunit and the mutated β_1 subunit were poorly expressed in cytosols, likely explaining the difference (Figure 2B). Unlike that of the WT, the maximal velocity of α_1/β_1M537N obtained at a saturating concentration of Glyco-SNAP-2 was not significantly increased when 100 μM YC-1 was added ($P > 0.1$). The enhanced basal and YC-1- and NO-stimulated catalytic activities are the result of an increase in the V_{max} of the reaction (K_m remaining roughly unchanged). In contrast, the combined presence of Glyco-SNAP-2 and YC-1 induced a strong decrease in the apparent K_m for GTP.

We then investigated how YC-1's capacity to enhance catalysis could be associated with a loss in YC-1's ability to increase maximal NO-stimulated activity (ratio of 1.0, Table 2a).

In α_1/β_1M537N, YC-1 Maintains the Ability To Increase NO Affinity but Lost the Capacity To Increase NO Efficacy. In comparison to the WT, this mutant displayed a stronger response to NO with a lower EC_{50} for activation by Glyco-SNAP-2 (Table 2b). When NO-stimulated activity was assessed in the presence of YC-1, the response curve to NO was shifted to the left (Figure 4). Nevertheless, only 100 μM YC-1 induced a significant decrease in the EC_{50} for NO, indicating that YC-1 maintained the ability to increase NO affinity, though higher concentrations were required. Most importantly, YC-1 at 10 or 100 μM lost the capacity to increase maximal NO-stimulated activity (Figure 4). There was no statistical difference between the plateau of the NO concentration−response curves in the absence and presence of YC-1 ($P > 0.1$). Thus, this mutation eliminates the effect of YC-1 on NO efficacy even though YC-1 alone still promotes a large increase in catalytic activity (inset of Figure 4).

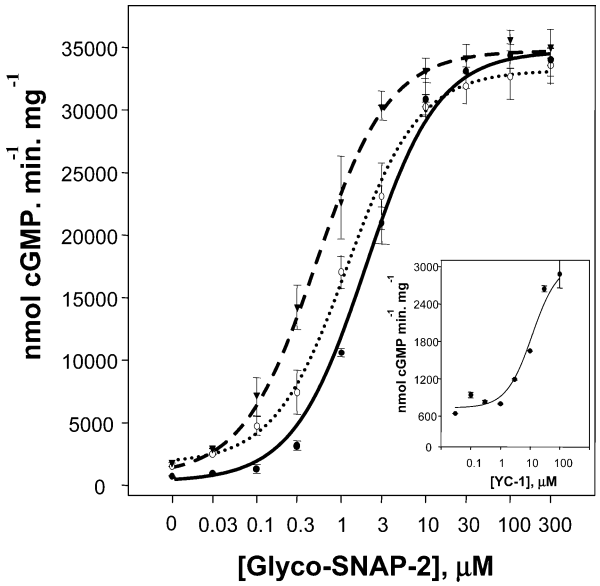

FIGURE 4: Glyco-SNAP-2 and YC-1 concentration−response curves of α_1/β_1M537N. The guanylyl cyclase activity of α_1/β_1-M537N was measured in the presence of increasing concentrations of Glyco-SNAP-2 or YC-1 (inset). Glyco-SNAP-2 concentration−response curves (●) were repeated in the presence of 10 (○) and 100 μM YC-1 (▼). Each experiment, carried out in duplicate, was repeated independently two or three times with two separate purified preparations, and results are the means ± the standard error of the mean of two experiments representative of these four to six independent experiments.

The WT Exhibits an Intermediate Phenotype: An Equilibrium Exists between Two Possible Interactions of YC-1 with the sGC Molecule. In each case, a single-point mutation blocks one YC-1 effect and allows or enhances the other effects, suggesting that YC-1 can interact in two different and independent ways with the sGC. If these two mutants actually illustrated two possible YC-1 interactions, the WT should exhibit an intermediate phenotype produced by both interactions. Indeed, kinetic analysis (Table 2b) showed that in the presence of 100 μM YC-1 the catalytic efficiency (V_{max}/K_m) of the WT was between each mutant value (10.6 vs 0.6 and 19 for α_1C594Y and β_1M537N, respectively), which was also true when 1 μM Glyco-SNAP-2 was added to YC-1 (catalytic efficiency of 203 vs 160 and 589 for α_1-C594Y and β_1M537N, respectively). Conversely, the V_{max} in the presence of 1 μM Glyco-SNAP-2 was increased 3.6-fold by addition of YC-1 in the WT, between the 11- and 2-fold increases for α_1C594Y and β_1M537N, respectively. The structural implications of these mechanistic findings are addressed in the discussion.

The Effect of BAY 41-2772 Is Similar to That of YC-1. We determined whether α_1C594Y/β_1 and α_1/β_1M537N displayed the same phenotypes in response to BAY 41-2272, which is structurally related to YC-1 (*36*) but was proposed to bind to the N-terminal region of α_1 (*11*). As shown in Figure 5, 10 μM BAY 41-2272 poorly activates α_1C594Y but induced a strong response in β_1M537N (left panel). In the presence of 100 μM Glyco-SNAP-2, BAY 41-2272 induced a remarkable increase in α_1C594Y catalytic activity and did not significantly increase β_1M537N activity (right panel). α_1C594Y and β_1M537N responses to BAY 41-2772 were identical with that to YC-1, suggesting that these two compounds have similar mechanisms of activation and that they likely interact at the same site of the sGC molecule.

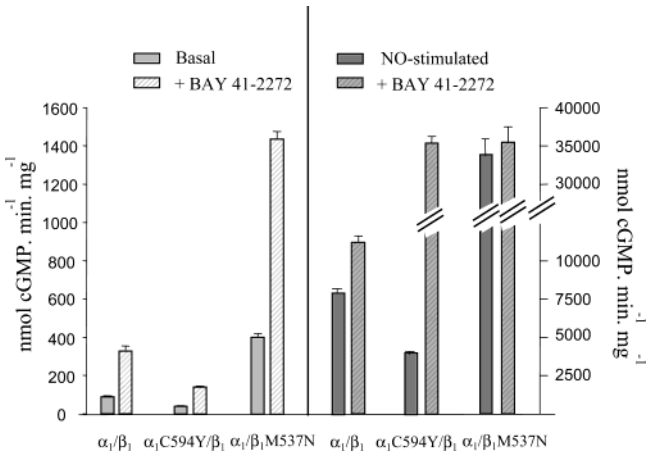

FIGURE 5: Effect of BAY 41-2272 on basal and NO-stimulated GC activity of the purified WT and mutants. GC activity was measured after addition of 10 μM BAY 41-2272 in the absence (left panel) or presence (right panel) of 100 μM Glyco-SNAP-2.

DISCUSSION

We used an analogy with ACs and the pseudosymmetric structure of sGC to conduct a comprehensive site-directed mutagenesis analysis. Initial screening of these mutants suggested that there must be a mechanism of synergistic activation in which the simultaneous binding of NO and YC-1 stimulates catalytic activity through a conformational change independent of the conformational change(s) induced by each activator alone.

In-depth kinetic analysis of the WT and two purified selected mutants (α_1C594Y/β_1 and α_1/β_1M537N) revealed that, in addition to the previously reported effect on NO affinity (*3*, *6*), YC-1 can affect the efficacy of NO stimulation. We found that a single-point mutation can dissociate the effect of YC-1 on NO affinity and NO efficacy. The α_1C594Y replacement in the pseudosymmetric pocket of sGC creates a mutant in which YC-1 lost the capacity to increase catalytic activity and affinity of NO for the heme but acquired an enhanced capacity to increase NO efficacy. This result suggested that YC-1 may have more than one mode of interaction with the sGC and that this mutation disfavors one mode of interaction and facilitates another one.

In a previous study, replacement of α_1C594 (C596 in bovine sequence) with a serine led to a mutant that displayed higher basal activity and a higher affinity for NO and responded to YC-1 but had no synergistic behavior (*17*). These opposite phenotypes first confirmed that α_1C594 is critical for YC-1's mechanisms of activation and second suggested that replacement with a serine favors another YC-1 interaction, which precludes synergy but enhanced individual activation. In both C594 mutants, the basal activity was changed, higher with a Ser at this position and lower with a Tyr, suggesting that C594 could participate in the conformation of the catalytic pocket.

The idea of two potential interactions of YC-1 with the sGC molecule was supported by the phenotypes generated by the β_1M537N replacement at the putative subunit interface. In a model reminiscent of the model of interaction between the C_1 and C_2 domains of AC, we anticipated β_1-M537 to have a function similar to that of C_2K1014. Indeed, α_1/β_1M537N displayed characteristics similar to the ones found in the AC mutant K1014N (*37*), such as a constitutively active phenotype and a strong response to activators, if we assume an analogy between YC-1 and FSK. We speculate that β_1M537N modifies the contacts at the interface like K1014N, inducing changes in the conformation of the catalytic pocket and in the propagation of activation. These changes generated a phenotype in which YC-1 maintains the capacity to increase catalytic activity and NO affinity but failed to enhance NO efficacy. Conversely, this mutation apparently favors a mode of interaction of YC-1 (through changes at the interface) that was abolished in the α_1C594Y/β_1 mutant and strikingly similar to the one reported in α_1-C596S/β_1.

These opposite phenotypes suggested that in the WT an equilibrium between two YC-1 interactions exists and that this equilibrium is affected by these mutations. Indeed, the WT exhibits an intermediate phenotype, as shown by kinetic analysis.

A structural explanation for these mechanistic findings would be that YC-1 interacts at two different sites of the sGC molecule or that YC-1 adopts two independent orientations in one site. The first possibility seems to be unlikely because a recent equilibrium dialysis study showed only one YC-1 binding site in the sGC (*38*). Thus, we investigate whether two different YC-1 orientations at one binding site could represent a possible structural explanation for the observed biochemical phenotypes.

Proposed Structural Model of YC-1's Interaction with the Catalytic Core of sGC. On the basis of the crystal structure of the catalytic core of AC, we and others have successfully used homology modeling to determine the catalytic mechanisms and substrate specificity of GCs (*14*, *27*, *39*). Using an analogous approach, and assuming that the site that is pseudosymmetric to the GTP binding site and analogous to the FSK site in AC is in fact the site that interacts with YC-1, we refined our previous structural model by docking YC-1 in this region. sGC amino acid sequences used for molecular modeling are the most conserved sequences among sGCs known to respond to YC-1 activation (*29*, *40*) and are most homologous to those of ACs (*13*).

After energy minimization, the model indicated that there are two favorable orientations of the YC-1 molecule (in yellow) in the pseudosymmetric pocket of sGC (Figure 6).

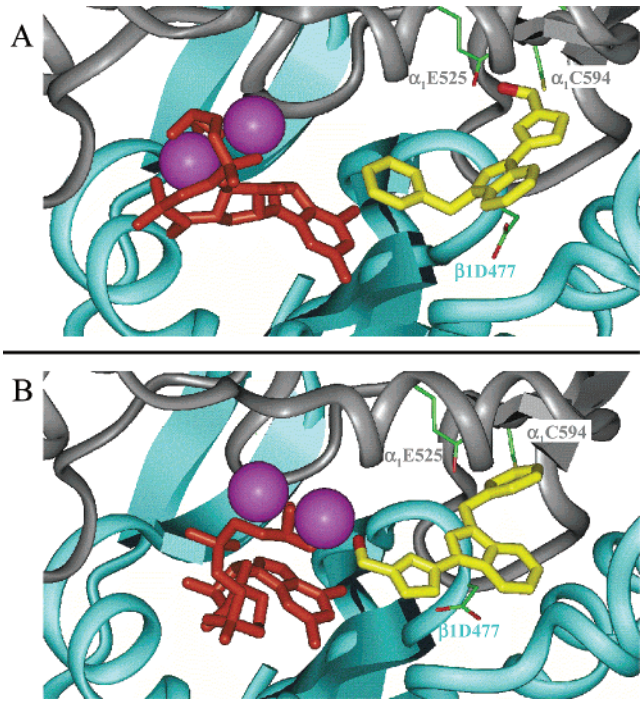

FIGURE 6: Two possible orientations of YC-1 in the catalytic core of sGC. α_1 and β_1 subunits are depicted in gray and cyan, respectively. For clarity, only the catalytic pocket is shown. Ligand YC-1, in yellow, and substrate GTP, in orange, are represented with thick sticks. Magnesium ions are shown as magenta spheres. O1 of the YC-1 hydroxyl is shown in red. Residues targeted at the sGC pseudosymmetric site are represented with thin sticks (α_1-C594, α_1E525, and β_1D477). (A) The YC-1 molecule is oriented such that its hydroxymethyl group is interacting with α_1C594 in the hydrophobic pocket of the sGC. (B) Another orientation of the YC-1 molecule with the hydroxymethyl group facing toward the substrate binding pocket. In this case, it contributes to the binding of a magnesium ion in the catalytic center.

In one orientation, the hydroxymethyl group (oxygen in red) of YC-1 is inside the hydrophobic pocket and the phenyl group is outside (Figure 6A). In the other orientation, the phenyl group is inside the pocket and the hydroxymethyl group faces the water outside the crevice (Figure 6B). The presence of two magnesium ions (in purple) in the modeling and their relative position in the catalytic pocket were based on an analogy with the two-metal ion catalysis of AC (*19*, *28*, *41*). Furthermore, a previous study showed that GC activity required two metal ions (*20*).

The crystal structure of YC-1 shows that O1 of the hydroxymethyl group can participate in molecular hydrogen bond formation (*26*). Thus, we speculate that in one orientation, this O1 forms a hydrogen bond with a serine or a cysteine of the sGC of the pseudosymmetric pocket (Figure 6A), and that in the other orientation it interacts with one of the magnesium ions of the substrate binding pocket (Figure 6B). In calculations, the orientation with O1 of YC-1 facing toward the magnesium ion (O1 outside, Figure 6B) was more favorable by ~1.5 kcal/mol than the orientation with the O1 inside (Figure 6A). In the orientation in Figure 6B, O1 of YC-1 likely interacts with the magnesium ion together with the γ-phosphate of GTP (in orange) and the oxygen of a residue in the vicinity. Consequently, in the orientation in Figure 6A, O1 of YC-1 potentially interacts with the sulfur of α_1C594.

Therefore, we propose that the equilibrium between two types of YC-1 interaction, suggested by our biochemical analysis, corresponds to an equilibrium between these two energetically close YC-1 orientations. We speculate that the mechanisms for the difference in activity between the two configurations could be related to the capacity of YC-1 to interact or not with the magnesium ion, which participates in the catalysis.

Another candidate site for YC-1 binding was recently proposed from a cross-linking study using a derivative of YC-1 (BAY 41-2272). The photolabile derivative of BAY 41-2272 labeled Cys238 and Cys243 in the N-terminal region of the α_1 subunit, and this labeling was inhibited by YC-1 (*11*). Our mutational analysis indicated that this region does not influence YC-1 activation. This is not entirely surprising as addition of a benzoylic spacer to generate the photolabile derivative of BAY 41-2272 created a distance of 9 Å between the photolabile azido group and the active core of the compound. This distance could have produced covalent labeling of the highly reactive Cys in a region not related to the YC-1 site. In addition, it is known that this region is poorly conserved in known mammalian α_1 subunit sequences (49.5% in this region vs 79.6% overall) and that Cys243 in the α_2 subunit of the YC-1-sensitive α_2/β_1 sGC is replaced with a proline. Moreover, a mutant carrying a deletion in the α_1 N-terminus that included this Cys region still exhibited responsiveness to YC-1 (*40*). We showed that BAY 41-2272 and YC-1 induced identical responses in α_1C594Y/β_1 and α_1/β_1M537N, suggesting a common site of interaction.

In conclusion, this study reveals the following. (1) YC-1 can increase *in vitro* NO efficacy in a manner that is independent of NO affinity. (2) The increase in NO-stimulated activity by YC-1 is due to an enhancement of both NO efficacy and affinity. (3) The effect on NO affinity and efficacy is dependent on an equilibrium between two types of interaction of YC-1 with the sGC. (4) Our refined structural model predicts that YC-1 can potentially bind in a site pseudosymmetric to the GTP catalytic site and equivalent to the FSK site of ACs. As a working hypothesis, we propose that YC-1 could accommodate two energetically close orientations in this site.

Recently published data obtained in a purified sGC system (*8*) and in cerebellar cells (*35*) showed that YC-1 became more potent with an increase in the NO concentration. Indeed, we showed that in the α_1C594Y/β_1 mutant low concentrations of NO induced a remarkable increase in YC-1-stimulated activity. Therefore, it is possible that NO controls the interaction of YC-1 with the catalytic pocket. The effect of NO on YC-1 occupancy and efficacy is currently under investigation.

The physiological relevance of these different modes of activation by YC-1 and NO has yet to be determined. Furthermore, an endogenous YC-1-like molecule has yet to be identified, in further analogy with AC and the unknown identity of the endogenous equivalent of FSK.

ACKNOWLEDGMENT

We thank Drs. A. Harris, S. Mukhopadhyay, and R. Sunahara for critical reading of the manuscript. We are grateful to Dr. Sylvain Rault for insightful discussion.

SUPPORTING INFORMATION AVAILABLE

Coomassie blue-stained SDS gel of purified sGC and selected mutants. This material is available free of charge via the Internet at http://pubs.acs.org.

REFERENCES

1. Wedel, B., Humbert, P., Harteneck, C., Foerster, J., Malkewitz, J., Bohme, E., Schultz, G., and Koesling, D. (1994) Mutation of His-105 in the beta 1 subunit yields a nitric oxide-insensitive form of soluble guanylyl cyclase, *Proc. Natl. Acad. Sci. U.S.A. 91*, 2592−2596.
2. Denninger, J. W., and Marletta, M. A. (1999) Guanylate cyclase and the NO/cGMP signaling pathway, *Biochim. Biophys. Acta 1411*, 334−350.
3. Koesling, D. (1999) Studying the structure and regulation of soluble guanylyl cyclase, *Methods 19*, 485−493.
4. Ignarro, L. J., Wood, K. S., and Wolin, M. S. (1982) Activation of purified soluble guanylate cyclase by protoporphyrin IX, *Proc. Natl. Acad. Sci. U.S.A. 79*, 2870−2873.
5. Kharitonov, V. G., Russwurm, M., Magde, D., Sharma, V. S., and Koesling, D. (1997) Dissociation of nitric oxide from soluble guanylate cyclase, *Biochem. Biophys. Res. Commun. 239*, 284−286.
6. Friebe, A., and Koesling, D. (1998) Mechanism of YC-1-induced activation of soluble guanylyl cyclase, *Mol. Pharmacol. 53*, 123−127.
7. Friebe, A., Schultz, G., and Koesling, D. (1996) Sensitizing soluble guanylyl cyclase to become a highly CO-sensitive enzyme, *EMBO J. 15*, 6863−6868.
8. Hoenicka, M., Becker, E. M., Apeler, H., Sirichoke, T., Schroder, H., Gerzer, R., and Stasch, J. P. (1999) Purified soluble guanylyl cyclase expressed in a baculovirus/Sf9 system: stimulation by YC-1, nitric oxide, and carbon monoxide, *J. Mol. Med. 77*, 14−23.
9. Martin, E., Lee, Y. C., and Murad, F. (2001) YC-1 activation of human soluble guanylyl cyclase has both heme-dependent and heme-independent components, *Proc. Natl. Acad. Sci. U.S.A. 98*, 12938−12942.
10. Mayer, B., and Koesling, D. (2001) cGMP signalling beyond nitric oxide, *Trends Pharmacol. Sci. 22*, 546−548.
11. Stasch, J. P., Becker, E. M., Alonso-Alija, C., Apeler, H., Dembowsky, K., Feurer, A., Gerzer, R., Minuth, T., Perzborn, E., Pleiss, U., Schroder, H., Schroeder, W., Stahl, E., Steinke, W., Straub, A., and Schramm, M. (2001) NO-independent regulatory site on soluble guanylate cyclase, *Nature 410*, 212−215.
12. Koglin, M., Stasch, J. P., and Behrends, S. (2002) BAY 41-2272 Activates Two Isoforms of Nitric Oxide-Sensitive Guanylyl Cyclase, *Biochem. Biophys. Res. Commun. 292*, 1057−1062.
13. Hurley, J. H. (1998) The adenylyl and guanylyl cyclase superfamily, *Curr. Opin. Struct. Biol. 8*, 770−777.
14. Liu, Y., Ruoho, A. E., Rao, V. D., and Hurley, J. H. (1997) Catalytic mechanism of the adenylyl and guanylyl cyclases: modeling and mutational analysis, *Proc. Natl. Acad. Sci. U.S.A. 94*, 13414−13419.
15. Tesmer, J. J., Sunahara, R. K., Gilman, A. G., and Sprang, S. R. (1997) Crystal structure of the catalytic domains of adenylyl cyclase in a complex with $G_{s\alpha}$·GTPγS, *Science 278*, 1907−1916.
16. Hurley, J. H. (1999) Structure, mechanism, and regulation of mammalian adenylyl cyclase, *J. Biol. Chem. 274*, 7599−7602.
17. Friebe, A., Russwurm, M., Mergia, E., and Koesling, D. (1999) A point-mutated guanylyl cyclase with features of the YC-1-stimulated enzyme: implications for the YC-1 binding site? *Biochemistry 38*, 15253−15257.
18. Kimura, H., and Murad, F. (1974) Evidence for two different forms of guanylate cyclase in rat heart, *J. Biol. Chem. 249*, 6910−6916.
19. Garbers, D. L., and Johnson, R. A. (1975) Metal and metal-ATP interactions with brain and cardiac adenylate cyclases, *J. Biol. Chem. 250*, 8449−8456.
20. Chrisman, T. D., Garbers, D. L., Parks, M. A., and Hardman, J. G. (1975) Characterization of particulate and soluble guanylate cyclases from rat lung, *J. Biol. Chem. 250*, 374−381.
21. Sunahara, R. K., Tesmer, J. J., Gilman, A. G., and Sprang, S. R. (1997) Crystal structure of the adenylyl cyclase activator Gsα, *Science 278*, 1943−1947.

22. Hatley, M. E., Benton, B. K., Xu, J., Manfredi, J. P., Gilman, A. G., and Sunahara, R. K. (2000) Isolation and characterization of constitutively active mutants of mammalian adenylyl cyclase, *J. Biol. Chem. 275*, 38626−38632.
23. Yuen, P. S., Doolittle, L. K., and Garbers, D. L. (1994) Dominant negative mutants of nitric oxide-sensitive guanylyl cyclase, *J. Biol. Chem. 269*, 791−793.
24. Domino, S. E., Tubb, D. J., and Garbers, D. L. (1991) Assay of guanylyl cyclase catalytic activity, *Methods Enzymol. 195*, 345−355.
25. Bradford, M. M. (1976) A rapid and sensitive method for the quantitation of microgram quantities of protein utilizing the principle of protein-dye binding, *Anal. Biochem. 72*, 248−254.
26. Sopkova-De Oliveira Santos, J., Collot, V., Bureau, I., and Rault, S. (2000) YC-1, an activation inductor of soluble guanylyl cyclase, *Acta Crystallogr. C56*, 1035−1036.
27. Sunahara, R. K., Beuve, A., Tesmer, J. J., Sprang, S. R., Garbers, D. L., and Gilman, A. G. (1998) Exchange of substrate and inhibitor specificities between adenylyl and guanylyl cyclases, *J. Biol. Chem. 273*, 16332−16338.
28. Zimmermann, G., Zhou, D., and Taussig, R. (1998) Mutations uncover a role for two magnesium ions in the catalytic mechanism of adenylyl cyclase, *J. Biol. Chem. 273*, 19650−19655.
29. Russwurm, M., and Koesling, D. (2002) Isoforms of NO-sensitive guanylyl cyclase, *Mol. Cell. Biochem. 230*, 159−164.
30. Bellamy, T. C., and Garthwaite, J. (2002) The receptor-like properties of nitric oxide-activated soluble guanylyl cyclase in intact cells, *Mol. Cell. Biochem. 230*, 165−176.
31. Friebe, A., Mullershausen, F., Smolenski, A., Walter, U., Schultz, G., and Koesling, D. (1998) YC-1 potentiates nitric oxide- and carbon monoxide-induced cyclic GMP effects in human platelets, *Mol. Pharmacol. 54*, 962−967.
32. Denninger, J. W., Schelvis, J. P., Brandish, P. E., Zhao, Y., Babcock, G. T., and Marletta, M. A. (2000) Interaction of soluble guanylate cyclase with YC-1: kinetic and resonance Raman studies, *Biochemistry 39*, 4191−4198.
33. Mulsch, A., Bauersachs, J., Schafer, A., Stasch, J. P., Kast, R., and Busse, R. (1997) Effect of YC-1, an NO-independent, superoxide-sensitive stimulator of soluble guanylyl cyclase, on smooth muscle responsiveness to nitrovasodilators, *Br. J. Pharmacol. 120*, 681−689.
34. Lee, Y. C., Martin, E., and Murad, F. (2000) Human recombinant soluble guanylyl cyclase: expression, purification, and regulation, *Proc. Natl. Acad. Sci. U.S.A. 97*, 10763−10768.
35. Bellamy, T. C., and Garthwaite, J. (2002) Pharmacology of the nitric oxide receptor, soluble guanylyl cyclase, in cerebellar cells, *Br. J. Pharmacol. 136*, 95−103.
36. Straub, A., Stasch, J. P., Alonso-Alija, C., Benet-Buchholz, J., Ducke, B., Feurer, A., and Furstner, C. (2001) NO-independent stimulators of soluble guanylate cyclase, *Bioorg. Med. Chem. Lett. 11*, 781−784.
37. Hatley, M. E., Gilman, A. G., and Sunahara, R. K. (2002) Expression, purification, and assay of cytosolic (catalytic) domains of membrane-bound mammalian adenylyl cyclases, *Methods Enzymol. 345*, 127−140.
38. Makino, R., Obayashi, E., Homma, N., Shiro, Y., and Hori, H. (2003) YC-1 facilitates release of the proximal His residue in the NO and CO complexes of soluble guanylate cyclase, *J. Biol. Chem. 278*, 11130−11137.
39. Tucker, C. L., Hurley, J. H., Miller, T. R., and Hurley, J. B. (1998) Two amino acid substitutions convert a guanylyl cyclase, RetGC-1, into an adenylyl cyclase, *Proc. Natl. Acad. Sci. U.S.A. 95*, 5993−5997.
40. Koglin, M., and Behrends, S. (2003) A functional domain of the alpha1 subunit of soluble guanylyl cyclase is necessary for activation of the enzyme by nitric oxide and YC-1 but is not involved in heme binding, *J. Biol. Chem. 278*, 12590−12597.
41. Tesmer, J. J., Sunahara, R. K., Johnson, R. A., Gosselin, G., Gilman, A. G., and Sprang, S. R. (1999) Two-metal-ion catalysis in adenylyl cyclase, *Science 285*, 756−760.

BI0360051